Antonio Soria-Verdugo[1], Elke Goos[2], Nestor García-Hernando[1], *Effect of the number of TGA curves employed on the biomass pyrolysis kinetics results obtained using the Distributed Activation Energy Model,* Fuel Processing Technology, Volume 134, June 2015, Pages 360–371.

[1] Carlos III University of Madrid (Spain), Energy Systems Engineering Group, Thermal and Fluids Engineering Department, Avda. de la Universidad 30, 28911 Leganés, Madrid, Spain

[2] Deutsches Zentrum für Luft- und Raumfahrt e.V. (DLR, German Aerospace Center), Institute of Combustion Technology, Pfaffenwaldring 38-40, 70569 Stuttgart, Germany

Effect of the number of TGA curves employed on the biomass pyrolysis kinetics results obtained using the Distributed Activation Energy Model

Antonio Soria-Verdugo[a]*, Elke Goos[b], Nestor García-Hernando[a]

[a] Carlos III University of Madrid (Spain), Energy Systems Engineering Group, Thermal and Fluids Engineering Department.

Avda. de la Universidad 30, 28911 Leganés (Madrid, Spain)

[b] Deutsches Zentrum für Luft- und Raumfahrt e.V (DLR, German Aerospace Center), Institute of Combustion Technology,

Pfaffenwaldring 38-40, 70569 Stuttgart (Germany)

* corresponding author: asoria@ing.uc3m.es Tel: +34916248884. Fax: +34916249430.

Abstract

The Distributed Activation Energy Model (DAEM) is widely used for determination of characteristic parameters of pyrolysis kinetics from a certain number of experimental thermal gravimetric analysis (TGA) curves obtained at different heating rates. The number of heating rates employed to obtain different TGA curves varies between different authors, being typically between 3 and 5. The validity of DAEM has been discussed by several authors based on its capability of describing the devolatilization kinetics of the samples. Nevertheless, to our knowledge, there are no studies available in the literature evaluating the uncertainties associated to the simplified DAEM method or quantifying the effect of considering different numbers of TGA curves in the analysis. Therefore, we studied the effect of the number of TGA curves considered in this work, as well as the effect of considering or neglecting the uncertainties of different measurement parameters employed in the calculation. The characterization was carried out using four types of biomass (pine wood, olive kernel, thistle flower and corncob) employing up to 9 different heating rates between 10 and 40 K/min during the TGA tests. Activation energies and pre-exponential factors were given and their uncertainties were reduced by increasing the number of TGA curves obtained at different heating rates. Nonetheless, considering measurement uncertainties during the calculations reduces significantly the final uncertainties of the pyrolysis parameters, permitting the reduction of the number of TGA curves used in the analysis.

Keywords: Distributed Activation Energy Model (DAEM), Biomass pyrolysis, Heating rate uncertainty, Temperature uncertainty, Thermal Gravimetric Analysis (TGA).

Nomenclature:

a Heating rate [K/s].

E_a Activation energy [J/mol].

k_0 Pre-exponential factor [s^{-1}].

R Universal gas constant [J/mol·K].

t Time [s].

T Temperature [K].

V Volatile mass loss [%].

V^* Volatile mass content [%].

V/V^* Reacted fraction [%].

1. Introduction

The characteristics of biomass as a primary energy source, such as its renewable character, wide distribution and almost carbon dioxide neutral emission, position biomass as an interesting alternative to fossil fuels. In fact, biomass is currently the fourth largest energy source in the world, supplying more than 14% of the total primary energy consumption in the world [1]. Biomass can be employed for power generation directly [2] or to produce desirable products such as liquid biofuels [3], synthesis gas [4], chemicals [5], and charcoal [6]. In most of these applications, biomass pyrolysis takes place as a first step in the biomass thermal decomposition.

The activation energy (E_a) and the pre-exponential factor (k_0) are the main parameters to describe biomass pyrolysis kinetics. Several models are available in the literature to establish the kinetics of pyrolysis, such as the single step model [7], the two parallel reaction model [8], the three pseudo-component model [9], the sectional approach model [10], and the Distributed Activation Energy Model (DAEM). DAEM was originally developed by Vand [11] and simplified later by Miura [12] and Miura and Maki [13] to obtain easily the activation energy and pre-exponential factor from several thermal gravimetric analysis (TGA) curves obtained at different heating rates. The method has been employed for a wide variety of samples, such as coal [13-15], charcoal [16], oil shale [17], polymers [18], medical waste [19], sewage sludge [20], and biomass [21-32]. The validity of DAEM was later discussed both experimentally [25] and theoretically [33].

Miura and Maki [13] proposed the use of three different heating rates TGA curves to determine the activation energy and the pre-exponential factor of the sample. Several other authors used three TGA curves in their works following this suggestion [20, 21, 23, 25, 28, 29, 34]. Other authors employed four [24, 26, 27, 30] or even five [15, 31] different heating rates TGA curves when applying DAEM to characterize the pyrolysis kinetics. Nevertheless, there are no studies concerning the effect of the number of different heating rates TGA curves employed in the calculation on the quality of the final results obtained. Furthermore, none of the works reported in the literature considered the uncertainties of the measurements of mass and temperature during the TGA test, or evaluated the final uncertainty associated to the results obtained after applying DAEM.

In this work, four different biomasses were tested (pine wood, olive kernel, thistle flower and corncob) in a TGA instrument employing several heating rates (10, 13, 16, 19, 22, 25, 30, 35 and 40 K/min). The uncertainties associated to the variables involved in the TGA tests (i.e. mass, temperature and heating rate) were evaluated based on the specifications of the manufacturer, and the effect of considering or neglecting these uncertainties on the final results for the pre-exponential factor and the activation energy of the devolatilization kinetics obtained employing DAEM was quantified. The effect of the number of TGA curves obtained at different heating rates employed in the calculation was also analysed, obtaining a large reduction of the uncertainty associated to the kinetic parameters when increasing the number of TGA curves employed during the calculation. Finally, a sensitivity analysis of the effect of the temperature accuracy on the final results was performed in order to extend the results obtained for different thermogravimetric analysers. The main objective of this work is to determine the effect of considering different number of TGA curves on the kinetic results obtained employing DAEM, and to analyse the effect of considering or neglecting the uncertainty of the input data during the calculation. Therefore, the DAEM methodology itself was assumed to be valid, and no uncertainty associated to the validity of the hypotheses imposed by the model was considered.

2. Experimental measurements

The thermogravimetric measurements were performed in a Thermogravimetric Analyser TGA Q500 from TA Instruments with a weighing precision of ±0.01% and sensitivity in the mass measurements of 0.1 µg. The baseline dynamic drift from 50 to 1000 °C at 20 K/min heating rate using empty platinum pans and no baseline subtraction method is lower than 50 µg. Its isothermal temperature accuracy was given as ±1 °C and its precision as ±0.1 °C. The measurements were carried out under an inert atmosphere, supplying the furnace a flow rate of 60 ml/min of nitrogen. As example, the resulting temperature profile with a heating rate of 10 K/min during the devolatilization process is shown in Fig. 1. First, the temperature was increased from room temperature to 105 °C, where an isothermal process during 20 min was carried out to dry the sample. Then, the temperature was reduced to 50 °C, and an increase in temperature at a constant heating rate was performed until 800 °C. The reduction of temperature to 50 °C and the heating up to 800 °C guaranteed a constant heating rate during the whole devolatilization process, between 150 °C and 500 °C for all samples investigated, without being interfered by the drying process of the sample. Finally, the temperature was stabilized at 800 °C prior to finalize the measurements. This temperature profile is better suited to obtain a constant heating rate during the devolatilization process than that employed in our previous works [20], [25], where the constant heating to devolatilize the sample started just after the drying process.
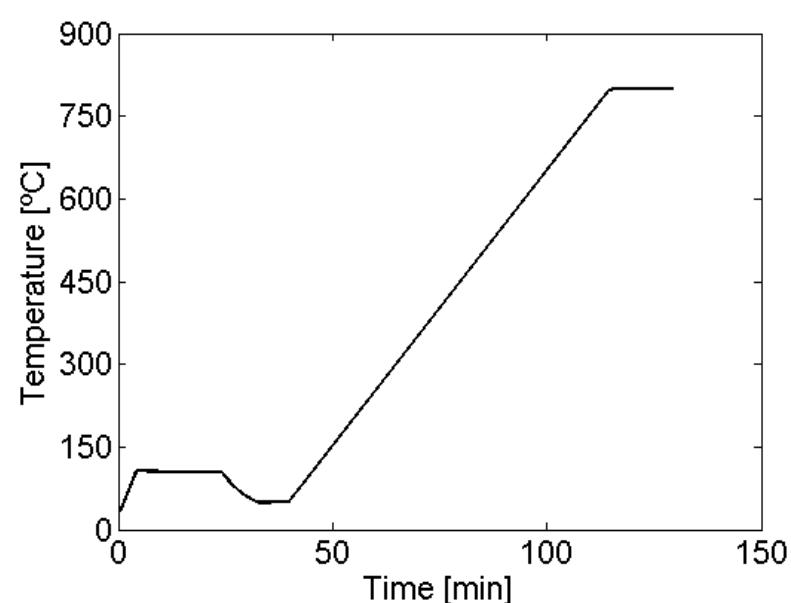
Fig. 1: Temperature profile employed in the TGA measurements (heating rate 10 K/min).

Four different biomasses were investigated: pine wood, olive kernel, thistle flower and corncob. In order to avoid heat transfer effects inside the samples during the measurements, the samples were shredded and sieved to a particle size under 100 µm, and the mass employed was around 10 mg (with a maximum deviation of ±0.5 mg) [21], [35]. A blank experiment was also run to exclude buoyancy effects [25]. The repeatability of the measurements was proven through repeating each measurement 3 times, obtaining relative differences for V/V* lower than 3% for the whole temperature range. The heating rate employed during the devolatilization process was either 10, 13, 16, 19, 22, 25, 30, 35 or 40 K/min to analyse the effect of the number of different TGA curves considered in the calculation of the pyrolysis kinetics parameters.

A proximate analysis of the samples was carried out in the thermogravimetric analyser TGA Q500 from TA Instruments, obtaining the volatiles content heating the samples up to 900 °C, employing a flow rate of 60 ml/min of nitrogen in the furnace. The ash content was determined as the remaining mass percentage after heating the samples up to 900 °C supplying the furnace with an oxygen flux of 60 ml/min. Finally, the fixed carbon content was determined by difference of the ash amount

and the volatiles amount from the dried sample mass. The results of the proximate analysis of the different samples can be found in Table 1.

The basic composition of the different biomasses was determined performing an analysis of the elemental composition in a LECO TruSpec CHN Macro and TruSpec S analyser. Therein Carbon, Hydrogen and Sulphur were detected by infrared absorption and Nitrogen was determined within a thermal conductivity cell. The results of these analyses are also shown in Table 1. The precision for the determination of the Carbon and Nitrogen content was ±0.5%, whereas for Hydrogen and Sulphur was 1%. The Oxygen content was obtained by difference, considering the Carbon, Hydrogen, Nitrogen, Sulphur and ash contents of the sample.

Table 1. Results of the proximate analysis and the elemental analysis (db: dry basis, [a] obtained by difference).

	Proximate analysis			
	Pine wood	Olive kernel	Thistle flower	Corncob
Volatiles [%db]	82.4	77.0	77.2	86,2
Fixed carbon[a] [%db]	14.3	20.6	18.4	11.1
Ashes [%db]	3.3	2.4	4.4	2.7
	Elemental analysis			
	Pine wood	Olive kernel	Thistle flower	Corncob
C [%db]	47.1	51.1	44.7	44.8
H [%db]	7.0	6.0	6.0	7.5
N [%db]	0.1	0.9	0.7	1.1
S [%db]	0.1	0.1	0.2	0.2
O[a] [%db]	42.4	39.5	44.0	43.7

The experiments were performed following the indications reported in the literature in order to obtain general results applicable to studies carried out by different authors.

3. Simplified DAEM

The Distributed Activation Energy Model was originally proposed by Vand (1943) [11]. DAEM is a multiple reaction model that assumes the devolatilization of a fuel to be composed of a large number of first order chemical reactions, occurring sequentially at determined activation energies. The velocity of the reaction is estimated using the Arrhenius kinetics equation for first order reactions. Therefore, the devolatilization process can be described in the integral form by Eq. 1:

$$1 - \frac{V}{V^*} = \int_0^\infty \exp\left(-k_0 \int_0^t e^{-E/RT} dt\right) f(E) dE \qquad (1)$$

where V/V^* is the reacted fraction, R the universal gas constant, T the temperature for each devolatilization process and $f(E)$ the distribution function of the activation energy.

The exponential function present in Eq. 1 is the so-called ϕ function, which can be transformed from an integral in time to an integral in temperature for a constant heating rate, a, as follows:

$$\phi(E,T) = \exp\left(-k_0 \int_0^t e^{-E/RT} dt\right) \cong \exp\left(-\frac{k_0}{a} \int_0^T e^{-E/RT} dT\right) \qquad (2)$$

The ϕ function can be approximated by a step function at a value of $E = E_a$, simplifying Eq. 1 to Eq. 3

$$V/V^* \cong 1 - \int_{E_a}^{\infty} f(E_a)dE_a = \int_0^{E_a} f(E_a)dE_a \qquad (3)$$

From Eq. 2, the ϕ function can be approximated to

$$\phi(E,T) \cong \exp\left(-\frac{k_0 RT^2}{aE}e^{-E/RT}\right) \qquad (4)$$

and selecting the value of the activation energy, E_a, to satisfy $\phi(E_a,T) = 0.58$ (a value found to obtain a proper approximation for many combinations of k_0 and $f(E)$ [12]), a relation between E_a, a, T and k_0 can be written (Eq. 5).

$$-\ln(0.58)\frac{aE_a}{k_0 RT^2} = e^{-E_a/RT} \qquad (5)$$

DAEM states that just one reaction with an associated activation energy, E_a, is taking place for a specified temperature, T, and heating rate, a. This idea can be written mathematically as

$$\frac{dV}{dt} \cong \frac{d(\Delta V)}{dt} = k_0 e^{-E_a/RT}\left(\Delta V^* - \Delta V\right) \qquad (6)$$

For a constant value of k_0, corresponding to a determined reaction, Eq. 6 can be integrated for a constant heating rate, a.

$$1 - \frac{\Delta V}{\Delta V^*} = \exp\left(-k_0 \int_0^t e^{-E_a/RT}dt\right) \cong \exp\left(-\frac{k_0 RT^2}{aE_a}e^{-E_a/RT}\right) \qquad (7)$$

which can be rewritten as

$$\ln\left(\frac{a}{T^2}\right) = \ln\left(\frac{k_0 R}{E_a}\right) - \ln\left[-\ln\left(1 - \frac{\Delta V}{\Delta V^*}\right)\right] - \frac{E_a}{R}\frac{1}{T} \qquad (8)$$

Looking at Eq. 7 we can set that $1 - \Delta V/\Delta V^* = \phi(E_a,T) = 0.58$. Therefore, Eq. 8 can be simplified to Eq. 9, which is the so-called Arrhenius equation of the DAEM that relates the main parameters of pyrolysis kinetics, the activation energy E_a and the pre-exponential factor k_0, with the heating rate a, for a determined temperature T.

$$\ln\left(\frac{a}{T^2}\right) = \ln\left(\frac{k_0 R}{E_a}\right) + 0.6075 - \frac{E_a}{R}\frac{1}{T} \qquad (9)$$

In view of Eq. 9, Miura and Maki [13] proposed a simple procedure to obtain the activation energy and pre-exponential factor of the sample.

First of all, V/V* is measured for three different heating rates, a, in a TGA instrument. Then, the Arrhenius plot is built, calculating and plotting $\ln(a/T^2)$ versus $1/T$ at selected values of V/V*. Finally, the activation energy, E_a, and the frequency factor, k_0, are determined from the slope, m, and intercept, n, in the Arrhenius plot for each V/V*. The relation of the activation energy and the pre-exponential factor with the slope and intercept of the Arrhenius plot (Eq. 10 and 11) can be obtained directly from Eq. 9:

$$E_a = -m \cdot R \qquad (10)$$

$$k_0 = -m \cdot \exp(n - 0.6075) \qquad (11)$$

4. Results and Discussion

Fig. 2 shows the reacted fraction V/V* as a function of temperature for the four samples (pine wood, olive kernel, thistle flower and corncob), obtained from the TGA curves. Devolatilization occurs between 150 ⁰C and 500 ⁰C for all the samples, obtaining a slight displacement of the devolatilization process to higher temperatures when increasing the heating rate, as an effect of the non-isothermal pyrolysis process [36], [37].

The behaviour of pine wood (Fig. 2a) and olive kernel (Fig. 2b) is quite similar, most of the devolatilization process occurs between 250 ⁰C and 350 ⁰C. For the thistle flower sample (Fig. 2c), the range of temperatures associated to devolatilization is wider, obtaining in this case a higher effect when varying the heating rate. The corncob sample (Fig. 2d) shows a sharp V/V* typical for carbohydrates such as starch, sucrose or cellulose. Notice that, the mass remaining after the devolatilization process, corresponding with the mass of fixed carbon and ashes, is different for all the samples (see Table 1).
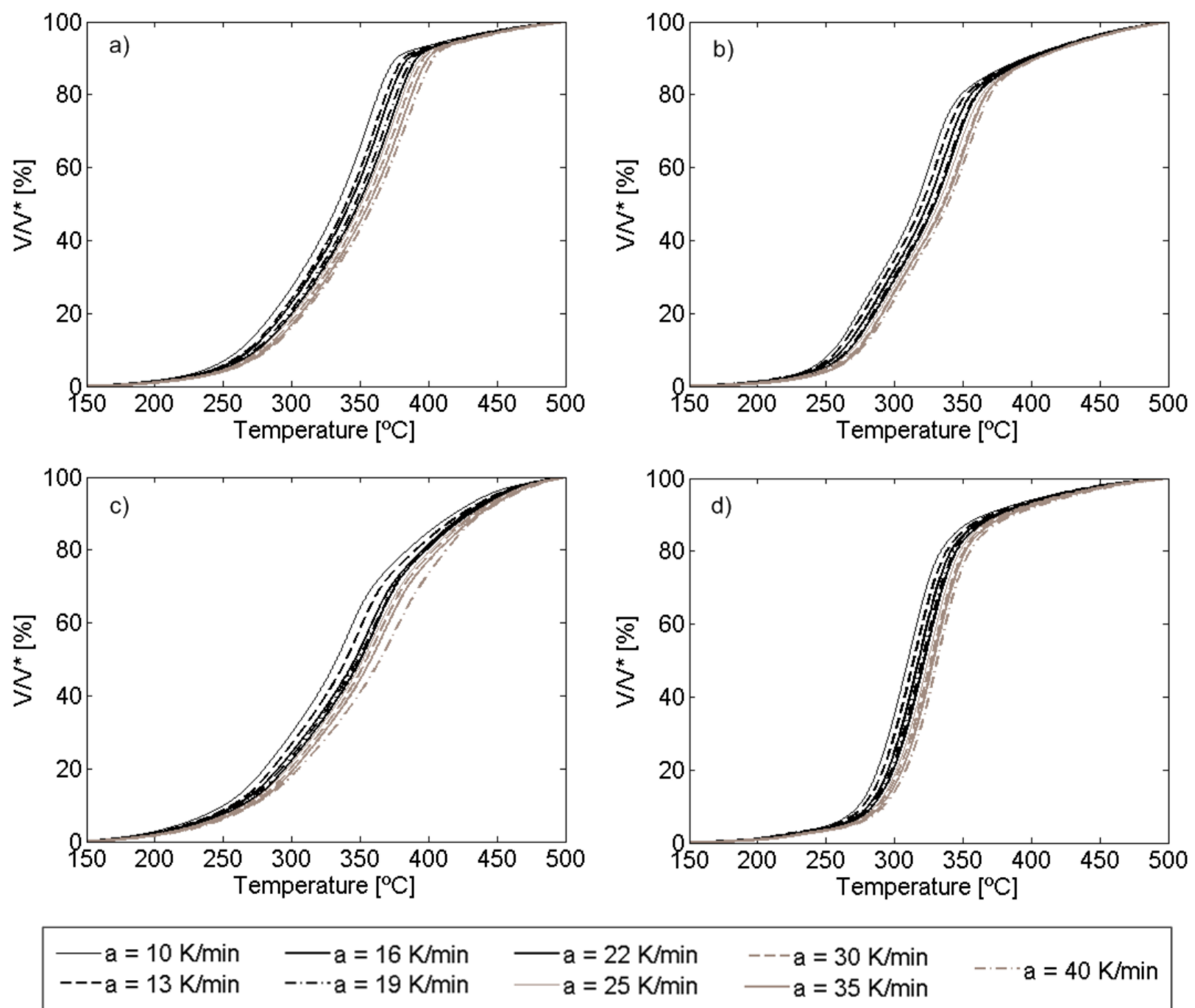
Fig. 2: Devolatilization curve for a) pine wood, b) olive kernel, c) thistle flower, and d) corncob.

The information concerning V/V*, shown in Fig. 2, can be employed to build the Arrhenius plot, which is shown in Fig. 3. The results obtained in the Arrhenius plot show a good linearity of the data for all the samples, as can be observed in Fig. 3. These data are usually linearized, employing typically three TGA curves obtained at three different heating rates, to determine the activation energy and the pre-exponential factor as stated above. Since the accuracy of TGAs is high both for the measurement of mass (weighing precision of ±0.01%, around 1 µg for a 10 mg sample) and for the temperature control (±1 ⁰C), no uncertainties are considered for the Arrhenius plot in the works reported in the literature. Nevertheless, even though

the uncertainties of the measurements are low, there is also an uncertainty associated to the method proposed by Miura and Maki [13] which might be of importance. Therefore, the uncertainties were considered in this work and their effect on the results obtained was discussed. The analysis of the uncertainties were carried out using the accuracy of the TGA Q500 TA Instruments employed to obtain the TGA curves, that is a weighing precision of ±0.01% and sensitivity in the mass measurements of 0.1 µg, as well as an isothermal temperature accuracy given as ±1 °C with a precision of ±0.1 ºC.
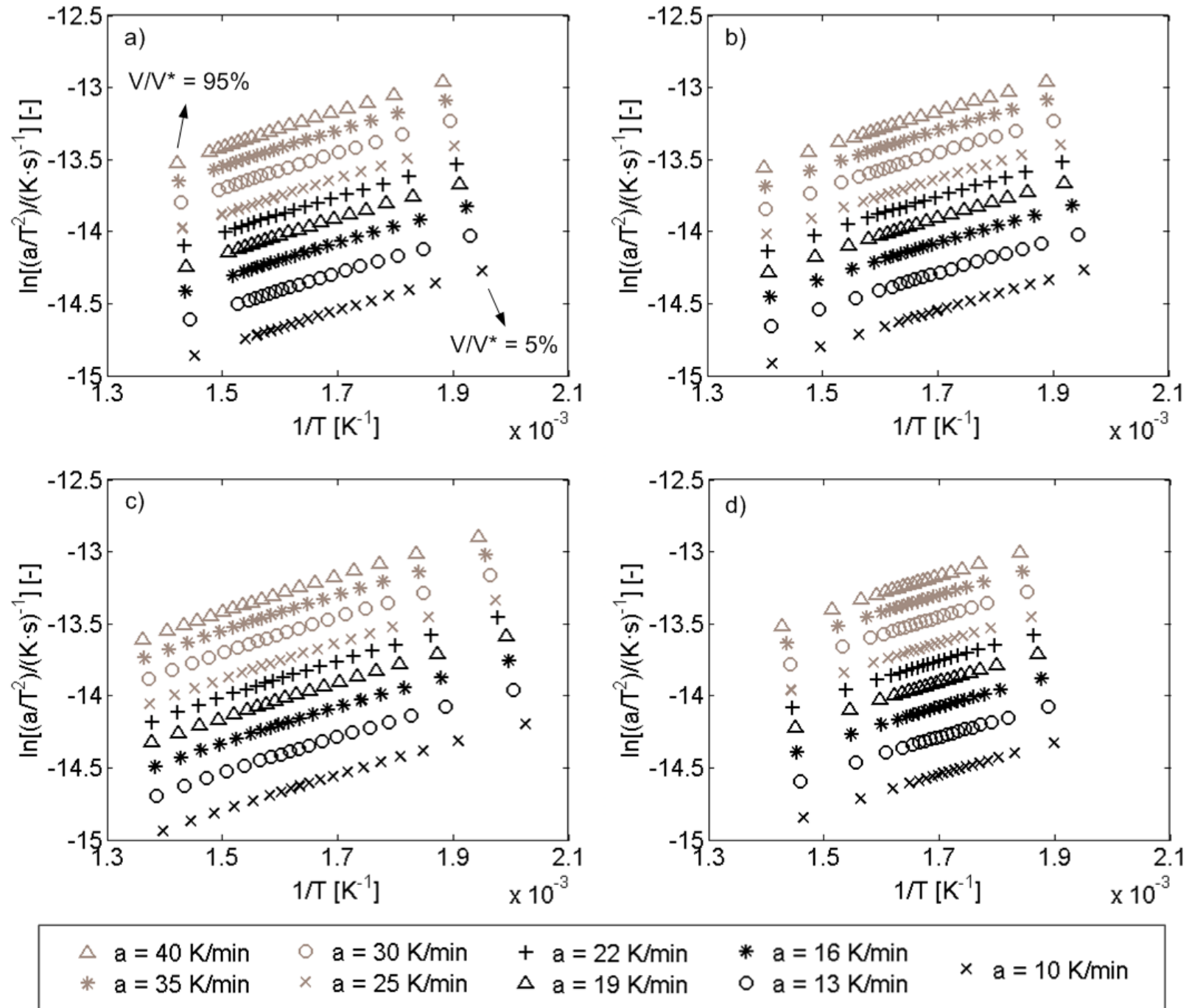
Fig. 3: Arrhenius plot for a) pine wood, b) olive kernel, c) thistle flower, and d) corncob.

In order to determine the uncertainty associated to the variables in the Arrhenius plot, both the uncertainty of the heating rate, a, and the temperature, T, must be analysed.

The heating rate is monitored during the TGA tests, thus the uncertainty can be determined as the difference between the nominal value provided to the TGA and the maximum deviation obtained during the devolatilization process (between 150 ºC and 500 ºC). The result is plotted in Fig. 4 for the different heating rates employed, obtaining a parabolic increase in the uncertainty when increasing the nominal value of the heating rate for all the cases. The parabolic increase of the uncertainty associated to the heating rate is properly described by Eq. 12,

$$\Delta a \; [K/\min] = 6.5 \cdot 10^{-4} \left(a \; [K/\min] \right)^2 - 1.5 \cdot 10^{-2} \left(a \; [K/\min] \right) + 0.13 \qquad (12),$$

obtaining a determination coefficient, R^2, between the experimental data and the parabolic fitting of 0.997. The maximum deviation of the heating rate was lower than 1.5% for all the cases, hence the simplified Distributed Activation Energy Model, which assumes a constant heating rate, can still be applied.
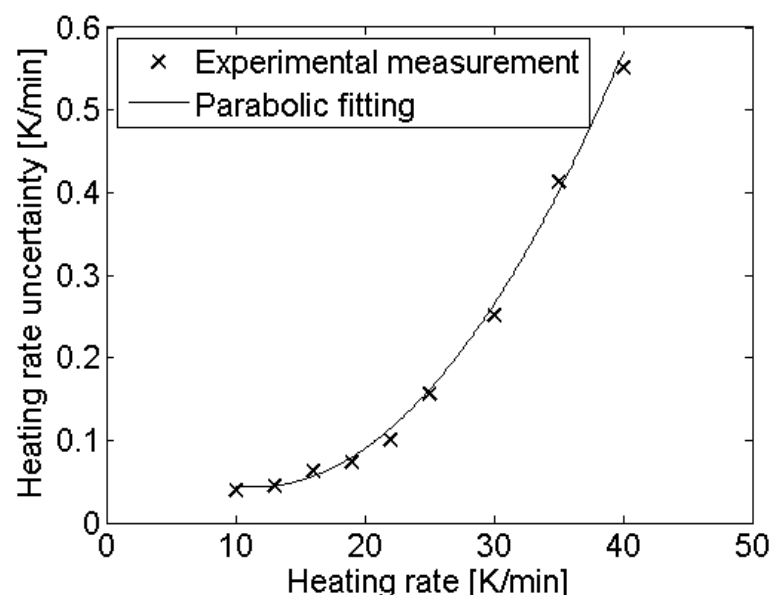
Fig. 4: Uncertainty associated to the heating rate.

The uncertainty associated with temperature in the Arrhenius plot can be attributed to two different causes. On the one hand, the temperature measured by the TGA counts on an uncertainty associated with the equipment, which in this case is ±1 °C. On the other hand, the determination of the temperature at which a determined V/V* takes place from Fig. 2, introduces two new sources of uncertainty. The uncertainty in the measurement of mass should be considered to determine the uncertainty associated to V/V*, and the effect of this uncertainty on the temperature determination will depend on the slope of the V/V* versus temperature curve. The uncertainty of V/V* was determined considering a variable uncertainty for the mass measurement during the measurement of ±0.01%, and checking that the uncertainty obtained is always higher than the device sensitivity (0.1 μg). These effects are shown graphically in Fig. 5 for the devolatilization of pine wood at 10 K/min. This figure shows the effect of the uncertainty of V/V* on the temperature in two zones of the devolatilization curve with a low slope (*V/V* = 3%* and *V/V* = 97%*) and in a zone of high slope (*V/V* = 50%*). The uncertainty associated to V/V* is amplified in the zones of low slope, whereas this effect is negligible for higher slopes. The three graphs showed in Fig. 5 present the same scale for both the x and y axis, so the effect of the slope of the devolatilization curve on the total uncertainty of the temperature can be appreciated visually. The uncertainty associated to the temperature in the Arrhenius plot is shown for all the values of V/V* in Fig. 6, for the pine wood sample at 10 K/min. The temperature uncertainty of the method is always higher than the uncertainty associated to the direct temperature measurement (±1 °C) due to the additional effect of the uncertainty of V/V*. For low and high values of V/V* the uncertainty of temperature is higher as a result of the lower slope in the devolatilization curve in these cases. For the determination of the uncertainty associated to the temperature, no variation between the measurement of the thermocouple of the TGA analyser and the real temperature of the sample was considered. However, the mass of the samples was selected to be low enough to reduce conduction effects according to the literature [21], [35].
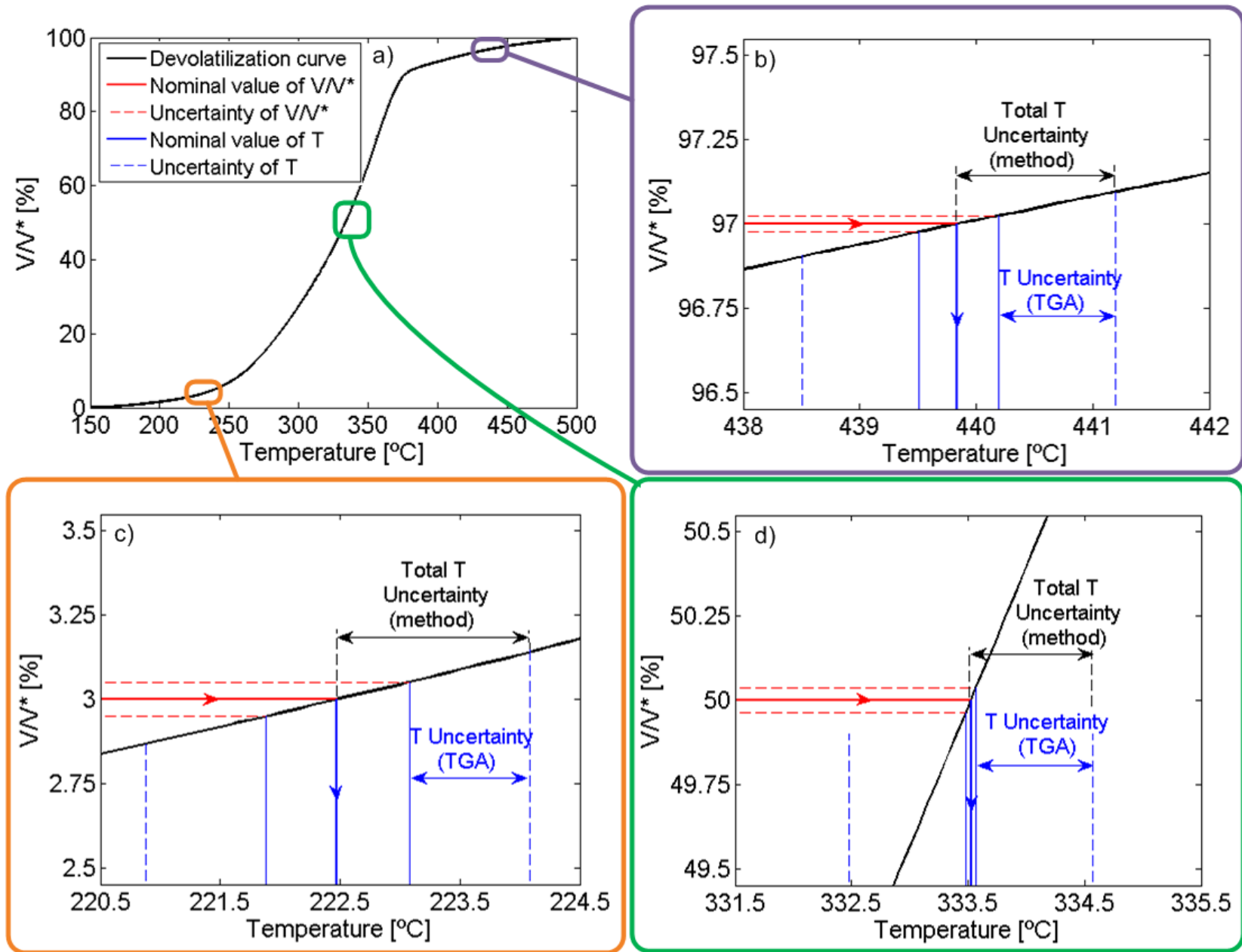
Fig. 5: Effect of the uncertainty of V/V* on the temperature determination a) Devolatilization curve, b) zoom for *V/V* = 97%*, c) zoom for *V/V* = 3%* and d) zoom for *V/V* = 50%*.
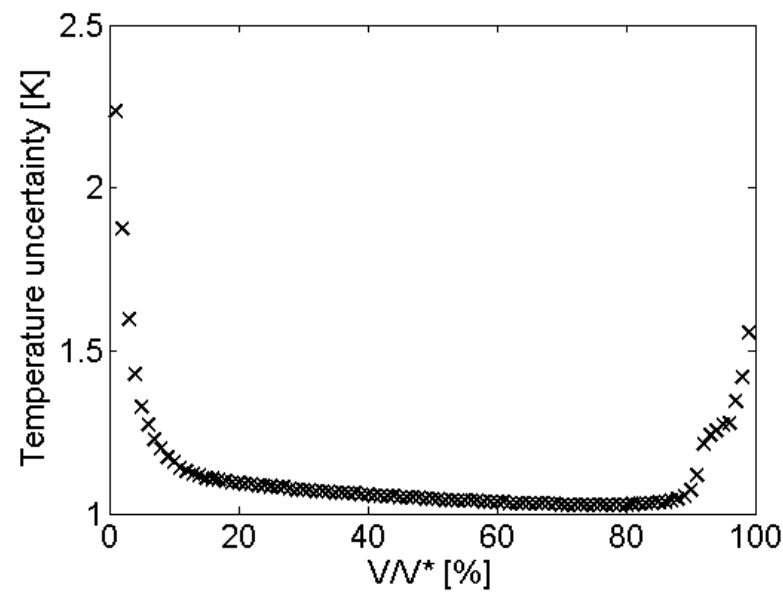
Fig. 6: Uncertainty associated to the temperature as a function of V/V* (pine wood sample at 10 K/min).

The consideration of these uncertainties in the linearization of the Arrhenius plot has a significant effect on the results obtained for the activation energy and the pre-exponential factor.

As an example, Fig. 7 shows the uncertainty of the activation energy for the pine wood sample, obtained from 3 TGA curves (*a = 10, 13, 16 K/min*) as proposed by Miura and Maki [13] and from 9 TGA curves (*a = 10, 13, 16, 19, 22, 25, 30, 35, 40 K/min*), considering and neglecting the uncertainties of *a* and *T*. In the case of neglecting the uncertainties of the heating rate and the temperature, the linearization was performed considering just the points presented in the Arrhenius plot, and the uncertainty of the activation energy was determined calculating the uncertainty of the linearization.

The linearization of the Arrhenius plot data was also carried out considering the uncertainties of both the heating rate and the temperature. The uncertainty obtained for the activation energy is notably lower when considering the uncertainties associated to the heating rate and the temperature, as can be observed in Fig. 7 for the pine wood sample. The mean activation energy for the pine sample was 165.0 kJ/mol and its lowest uncertainty of ±0.95% was reached for V/V^* values between 20% and 70% by considering the uncertainties of 9 TGA curves. For the total range of all V/V^* values, the maximal uncertainty for the activation energy E_a was ±1.55% by considering the uncertainties of 9 TGA curves.

When neglecting the uncertainties of the input data in the calculation, the uncertainty obtained for the activation energy is a function of the linearity of the data in the Arrhenius plot (Fig. 3), which can be improved by adding more TGA curves obtained at different heating rates in the analysis. On the other hand, when considering the uncertainties in the calculation, the value obtained for the activation energy is more accurate, obtaining a slightly higher uncertainty in this case for low and high values of V/V* as a consequence of the higher uncertainty associated to the temperature in this zone, as shown in Fig. 6.
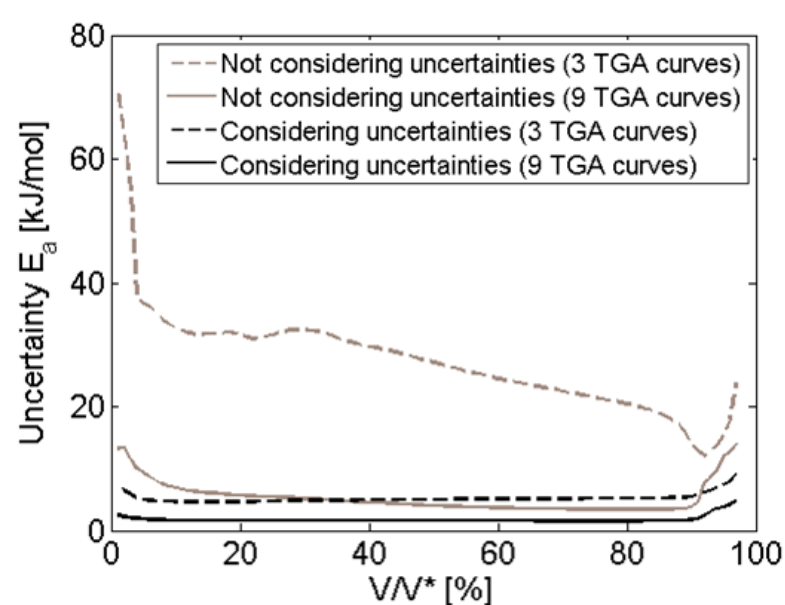
Fig. 7: Activation energy uncertainty of the pine wood sample.

The accuracy of the linearization of the data in the Arrhenius plot was studied, analysing both the effect of considering or neglecting the uncertainties of the heating rate and the temperature and the effect of the number of different heating rates TGA curves employed in the linearization. The minimum number of curves considered was three (10, 13, and 16 K/min), as suggested originally by Miura and Maki [13], and then curves obtained at higher heating rates were added up to a maximum of nine curves (10, 13, 16, 19, 22, 25, 30, 35, 40 K/min). The results obtained for the mean uncertainty of the slope, m, and the intercept, n, of the linearization are shown in Fig. 8 as a function of the number of curves employed, considering and neglecting the uncertainties of the parameters present in the Arrhenius plot. It can be observed that there is a considerable difference in the mean uncertainty of both the slope and the intercept of the linearization due to the consideration of the uncertainties of the parameters involved in the analysis. Considering the uncertainties associated to the heating rate and the temperature reduce significantly the uncertainty of the slope and the intercept of the Arrhenius plot, concluding in a more accurate determination of the activation energy and the pre-exponential factor for any number of curves employed. Nevertheless, when neglecting the uncertainties of the heating rate a and temperature T, the accuracy in the determination of the slope and the intercept is discussible for a low number of curves employed. The accuracy of these parameters, and therefore the accuracy in the determination of the activation energy and the pre-exponential factor can be improved in this case through increasing the number of curves considered. A total number of 6 different heating rates TGA curves is needed when neglecting the uncertainties of the heating rate and the temperature in order to obtain mean uncertainties lower than

15% for the slope and intercept in all the samples tested. However, considering the uncertainties of a and T during the linearization of the Arrhenius plot data leads to mean uncertainties lower than 15% for m and n even when employing just 3 different heating rates TGA curves for the linearization. Therefore, the consideration of uncertainties of the input data during the calculation improves significantly the accuracy in the determination of the characteristic parameters of the biomass pyrolysis, the activation energy and the pre-exponential factor. Furthermore, considering the uncertainties in the calculation permits the use of a low number of TGA curves for the analysis. Considering 9 TGA curves obtained at different heating rates, the maximum number of curves investigated for each sample in this work, decreases the uncertainty of m and n to values lower than 2.1% and 3.2%, respectively, for all four biomass samples investigated.
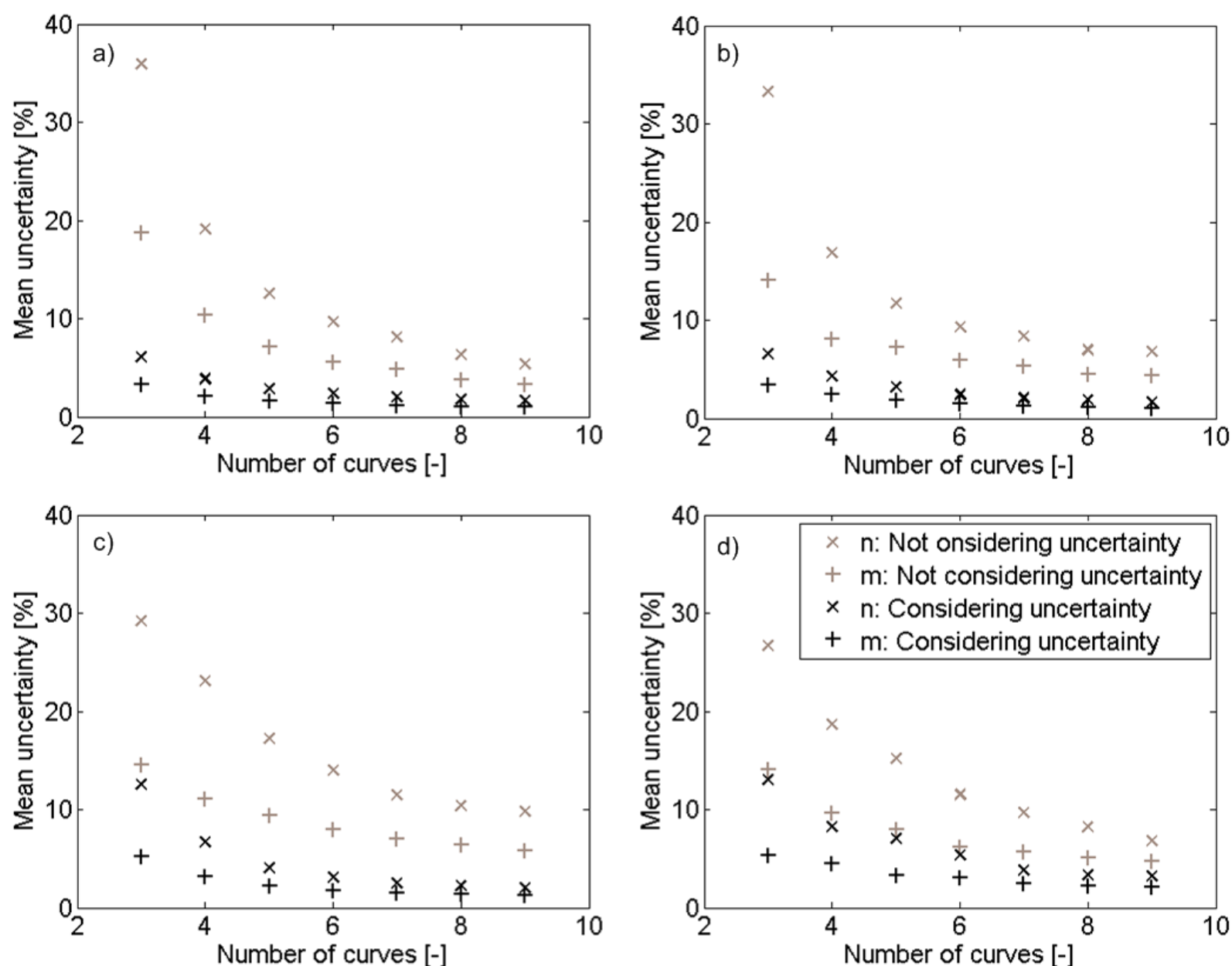
Fig. 8: Mean uncertainty of the slope m and intercept n of the Arrhenius plot data linearization as a function of the number of curves employed, a) pine wood, b) olive kernel, c) thistle flower, and d) corncob.

Finally, the main parameters of the pyrolysis kinetics of the biomass samples, the activation energy E_a and the pre-exponential factor k_0, were obtained for the most accurate case, that is considering the uncertainties during the calculation and employing 9 different heating rates TGA curves. The results obtained for all the samples are shown in Fig. 9. A similar trend is observed for both the activation energy (Fig. 9a) and the pre-exponential factor (Fig. 9b) for all the samples, showing a uniform value for a wide variation of V/V* and a sharp increase for high values of V/V*. The kinetic parameters obtained in our work for the pine sample are in agreement with those of [24, 30, 38-40], the values for the olive kernel sample are similar to those obtained by [41-43], the activation energy and pre-exponential factor of the thistle flower sample are comparable to the values reported by [44], and the results obtained for the corncob sample are similar to those of [23, 27, 45].

The mean activation energy for the uniform zone between V/V*=20% and V/V*=70% are for pine wood 165.0 kJ/mol, for olive kernel 162.2 kJ/mol, for thistle flower 154.5 kJ/mol, and for corncob sample 183.5 kJ/mol. The pre-exponential factor for the 4 samples are respectively $1.6 \cdot 10^{12}$ s^{-1}, $4.1 \cdot 10^{12}$ s^{-1}, $2.8 \cdot 10^{11}$ s^{-1} and $2.3 \cdot 10^{14}$ s^{-1}.

Once the activation energy and the pre-exponential factor are determined, the reaction rate coefficient can be obtained according to Eq. 13, solving Eq. 9 through a Newton-Raphson method to find the actual temperature.

$$k = k_0 e^{-E/RT} \tag{13}$$

The results are shown in Fig. 9c for the different samples, obtaining a similar tendency to that of the activation energy and the pre-exponential factor, with a uniform value for a wide range of V/V* and increasing values at the end of the devolatilization process. The resulting first order reaction rate for the devolatilization process of solid samples are for pine wood $5.0 \cdot 10^{-3}$ s^{-1}, for olive kernel $5.3 \cdot 10^{-3}$ s^{-1}, for thistle flower $4.7 \cdot 10^{-3}$ s^{-1}, and for corncob $6.0 \cdot 10^{-3}$ s^{-1}, for values of V/V* between 20% and 70%. In the temperature range investigated, their order of magnitude is in agreement with kinetic data set used for modelling of cellulose degradation during a pyrolysis process [10].
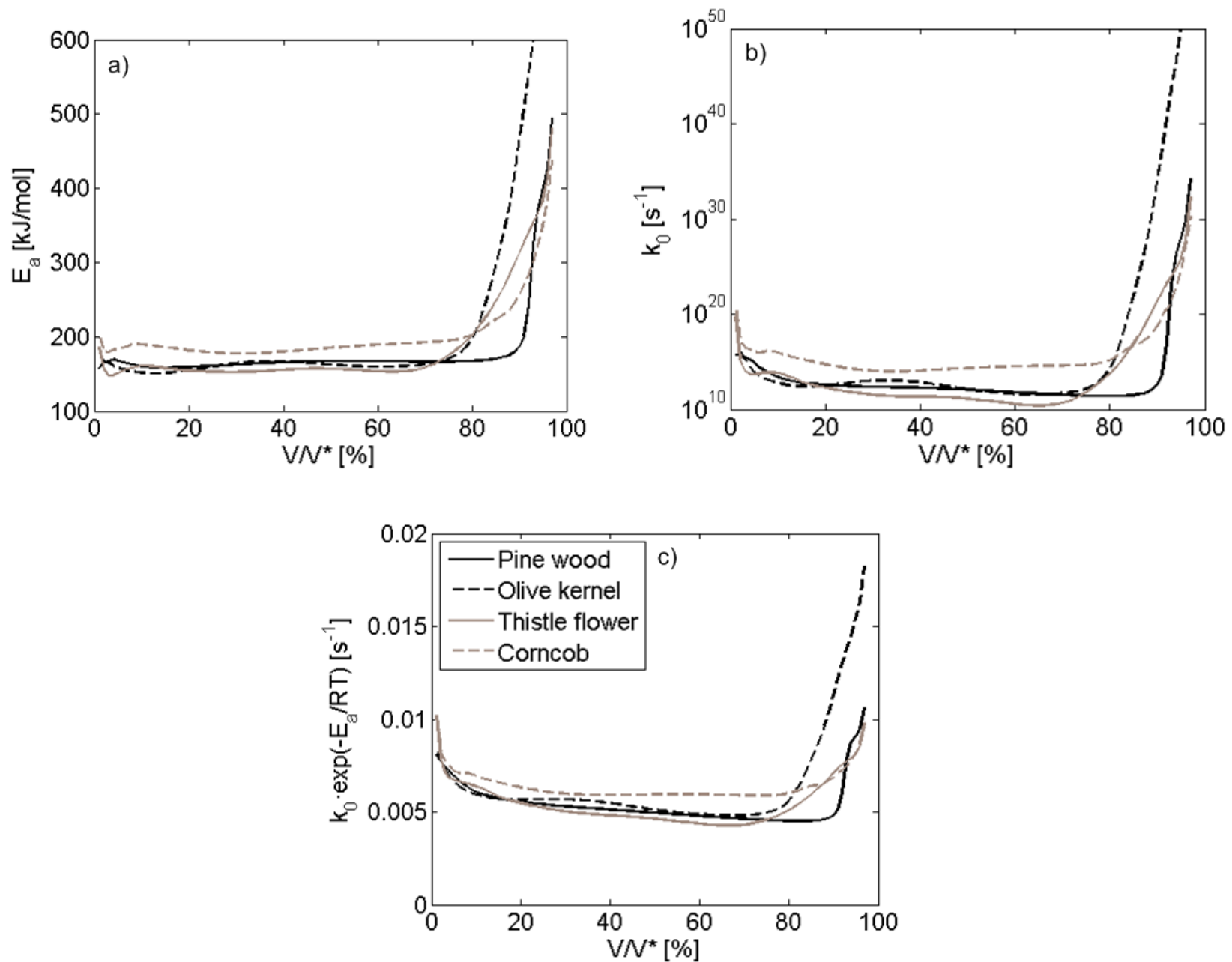
Fig. 9: Pyrolysis kinetic parameters of the biomass samples obtained employing 9 TGA curves considering the uncertainties: a) activation energy E_a b) pre-exponential factor k_0 c) first order reaction rate of the different samples.

The uncertainties associated to the values of the activation energy and the pre-exponential factor shown in Fig. 9 can be obtained from Eq. 10 and 11 applying the error propagation. The expression of the uncertainties of the activation energy and pre-exponential factor in percentage are shown in Eq. 14 and 15 respectively.

$$\frac{\Delta E_a}{E_a} = \frac{\Delta m}{m} \qquad (14)$$

$$\frac{\Delta k_0}{k_0} = \frac{\Delta m}{m} + \Delta n \qquad (15)$$

The uncertainty associated to the activation energy in percentage is just that of the slope m shown in Fig. 8, whereas the uncertainty associated to the pre-exponential factor is much higher, as shown in Fig. 10.
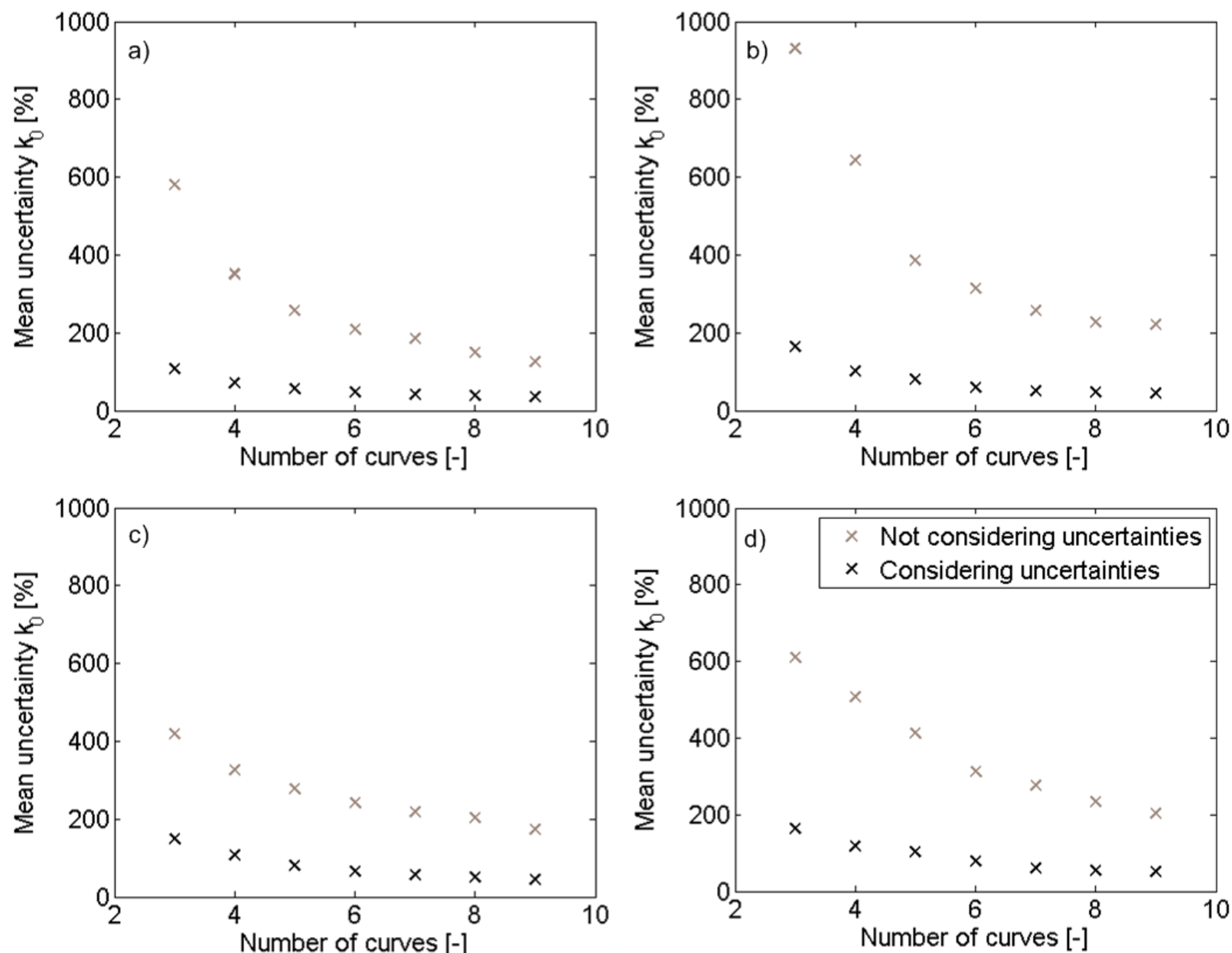
Fig. 10: Mean uncertainty of the pre-exponential factor as a function of the number of curves employed, a) pine wood, b) olive kernel, c) thistle flower, and d) corncob.

The lowest mean uncertainties of the activation energy, reached within this investigation with 9 different heating rates TGA curves, were 0.97% for pine wood, 1.04% for olive kernel, 1.20% for thistle flower, and 2.10% for corncob, and 35.3%, 44.4%, 44.0%, and 51.3% respectively for the pre-exponential factor of the 4 different samples, resulting in the following values, given in Table 2, for a temperature precision and therefore uncertainty of the TGA device of ±1.0 °C. Notice that these uncertainties were determined considering just the accuracy of the mass and temperature measurements obtained from the specifications of the TGA analyser manufacturer and determining the uncertainty of the heating rate, but no uncertainties derived from the validity of the hypotheses assumed by the model were considered in order to facilitate the comparison of the results obtained using different number of TGA curves or considering or neglecting the uncertainties of the input data. The consideration of the effect of these hypotheses would lead to higher uncertainties for the activation energy and pre-exponential factor.

Table 2: Mean values and uncertainties for the activation energy and the pre-exponential factor obtained for values of V/V* between 20% and 70%. The data was obtained using 9 TGA curves and considering the uncertainties, under a temperature accuracy and therefore uncertainty of the TGA device of ±1.0 °C.

	Mean Uncertainty of Activation Energy [%]		Mean Uncertainty of Pre-exponential Factor [%]	
	$\Delta T = 2°C$	$\Delta T = 0.5°C$	$\Delta T = 2°C$	$\Delta T = 0.5°C$
Pine wood	1.26	0.69	45.65	25.34
Olive kernel	1.33	0.76	56.95	35.73
Thistle flower	1.55	0.87	56.06	32.22
Corncob	2.45	1.82	60.96	43.30

The values of the activation energy and the pre-exponential factor obtained using DAEM were analysed to investigate the existence of the compensation effect. According to Barrie [46], the kinetic compensation effect occurs when there is a linear relation between $\ln(k_0)$ and E_a, in the form of Eq. 16.

$$\ln\left(k_0/s^{-1}\right) = \alpha + \beta \cdot E_a \qquad (16)$$

where α and β are constants.

Fig. 11 shows the values of $\ln(k_0)$ as a function of E_a for each biomass sample, together with the correlation described by Eq. 16 for high values of V/V*. The values and tendencies obtained for the different samples are similar to those reported by Sonoyama and Hayashi [47] for sugarcane, pine sawdust, cedar sawdust and coffee residue and to the results of Li et al. [9] for corn stalk. The values of the constants α and β showed in of Eq. 16 are reported in Table 3 for high values of V/V*, together with the determination coefficient R^2 of the fitting of the experimental data with Eq. 16, for the four types of biomasses analysed in our work.

Table 3: Values of the constants for the linearization of the compensation plots.

	α [-]	β [mol/kJ]	R^2 [-]
Pine wood	-1.07	0.164	0.9989
Olive kernel	-1.20	0.174	0.9995
Thistle flower	0.18	0.155	0.9996
Corncob	5.84	0.146	0.9991

In view of the high values of the determination coefficient obtained for all the samples, it can be concluded that there is a kinetic compensation effect in this case. This is in accordance with several previous works concerning biomass pyrolysis reported in the literature [9, 47-51].
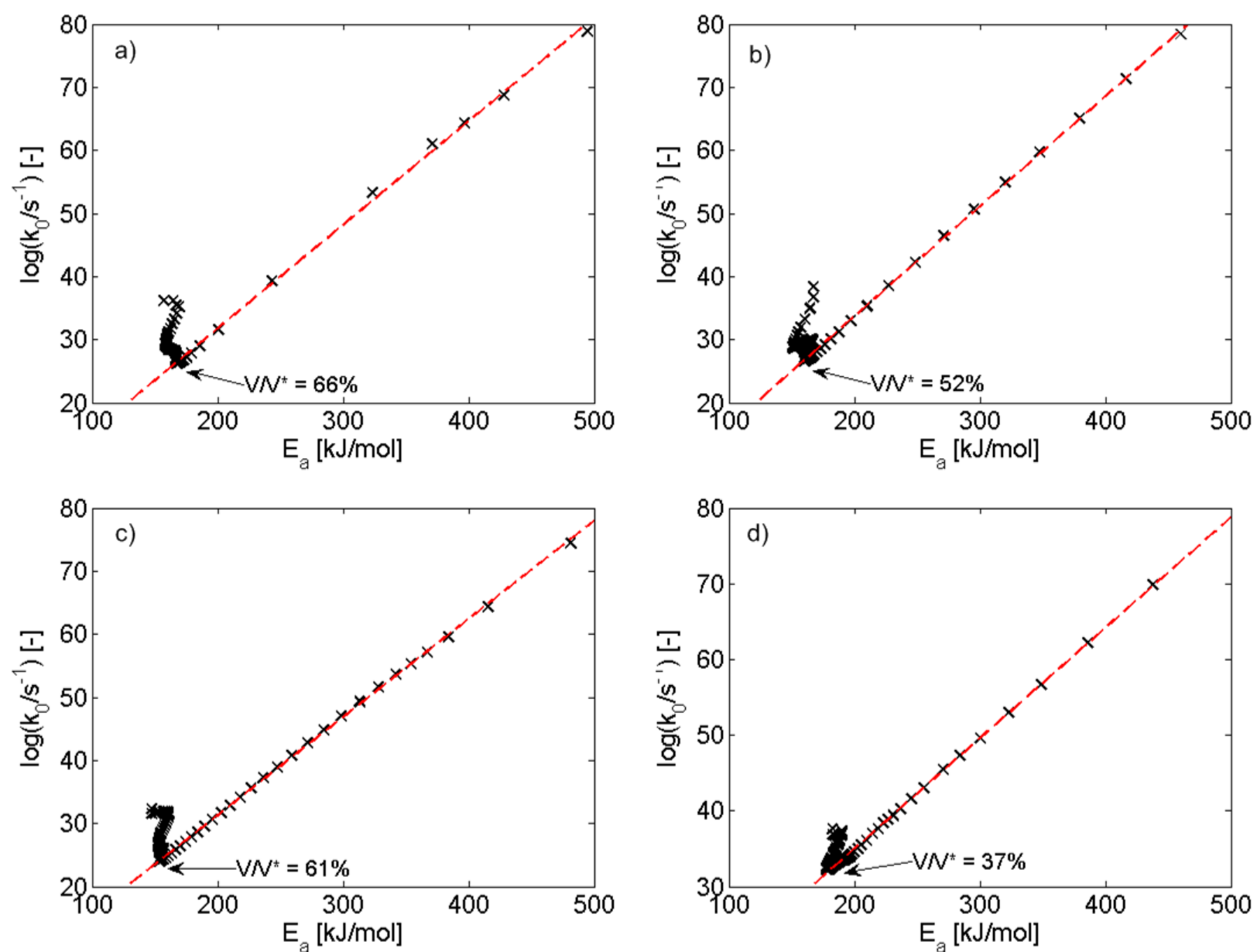
Fig. 11: Compensation plot, a) pine wood, b) olive kernel, c) thistle flower, and d) corncob.

The results obtained for the uncertainties of both the activation energy and the pre-exponential factor depend on the thermogravimetric analyser employed, since the accuracy of the mass and temperature measurements and the uncertainty of the heating rate were imposed. The accuracy of the temperature measurement is the most variable parameter between different devices and it is also the parameter with the highest effect on the results. The temperature accuracy can vary for different devices from 2 °C for the thermo gravimetric analyser Pyris 1 TGA (PerkinElmer) to just 0.1 °C for a couple gas analyser SENSYS evo TG-DSC (SETARAM Instruments). Therefore, a sensitivity analysis was carried out to study the influence of the accuracy of the temperature determination on the final results, in order to extend the results obtained to different thermo balances. The sensitivity analysis was performed for the four samples, obtaining the uncertainties of the activation energy and the pre-exponential factor for temperature accuracies of 2, 1, 0.5 and 0.1 °C. The results are shown in Fig. 12, where a direct effect of the temperature accuracy on the uncertainties obtained can be observed.

Fig 12 shows a reduction of the mean uncertainty of both the activation energy and the pre-exponential factor when employing a thermo gravimetric device with a higher accuracy for the measurement of temperature. The differences obtained for different analysers are higher when employing a low number of different heating rates TGA curves in the analysis, but they are still important when using 9 TGA curves obtained at different heating rates.
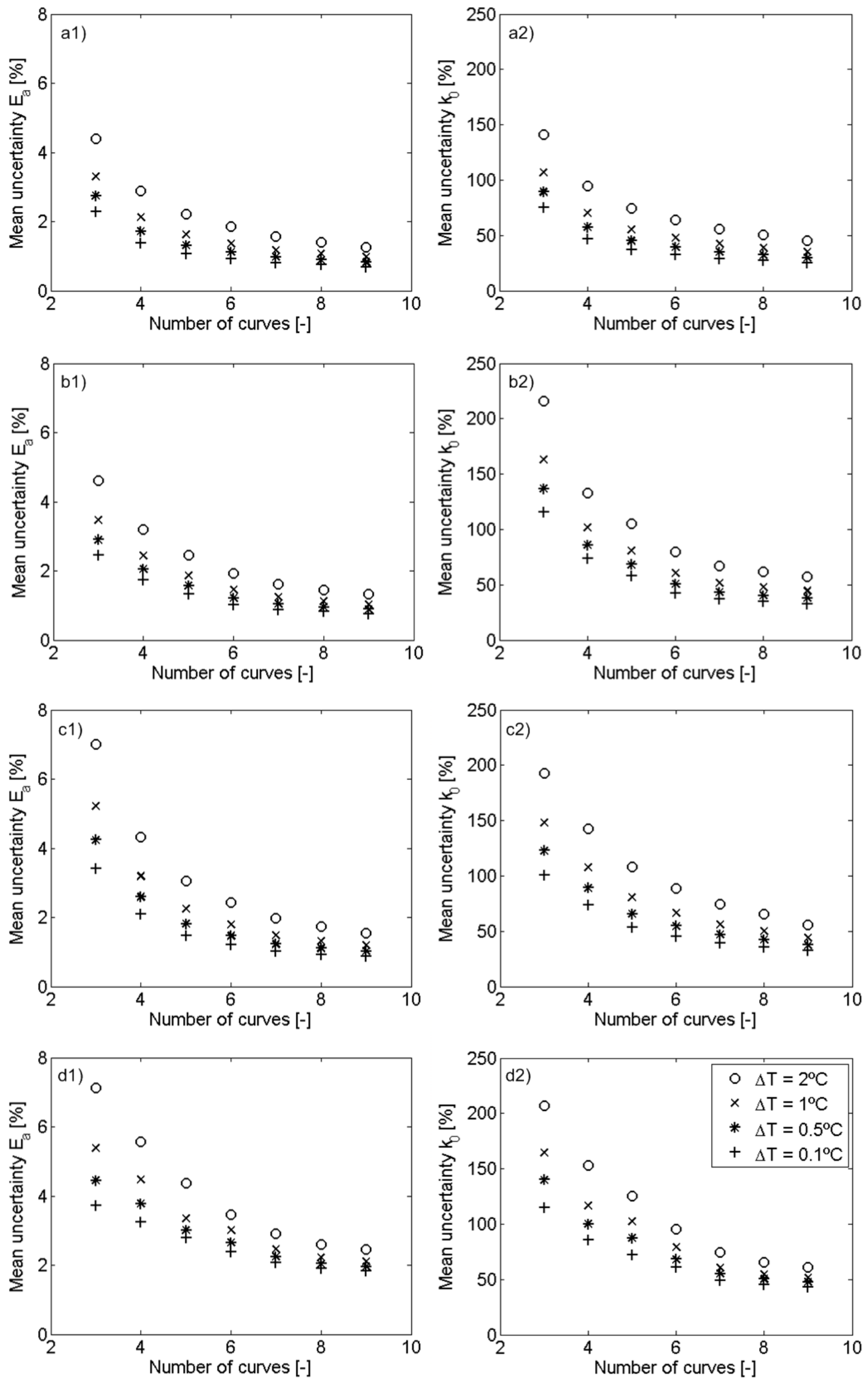
Fig. 12: Mean uncertainty of the activation energy (left) and pre-exponential factor (right) as a function of the number of curves employed for various temperature accuracies, a) pine wood, b) olive kernel, c) thistle flower, and d) corncob.

5. Conclusions

Four different types of biomass (pine wood, olive kernel, thistle flower and corncob) were analysed experimentally in a TGA at different heating rates (10, 13, 16, 19, 22, 25, 30 35, 40 K/min). The simplified Distribution Activation Energy Model was applied to obtain the main parameters of the pyrolysis kinetics (activation energy and pre-exponential factor) from the linearization of the Arrhenius plot. The uncertainties associated to the temperature and mass measurements were deduced based on the accuracy reported by the thermo gravimetric analyser manufacturer, whereas the uncertainty associated to the heating rates was directly measured during the tests. The uncertainty associated to the heating rate was found to be higher when increasing the heating rate value, following a parabolic law, whereas the uncertainty associated to the temperature was found to be strongly dependent on the slope of the devolatilization curve.

The effect of considering or neglecting the uncertainties of the heating rate and the temperature during the calculation on the accuracy of the linearization was quantified, and the effect of the number of TGA curves employed during the linearization was also studied. The uncertainty associated to the slope and intercept of the linearization of the Arrhenius plot data was found to decrease significantly when considering the uncertainties of the heating rate and temperature. When neglecting the uncertainties of the heating rate and the temperature, the uncertainty associated to the slope and the intercept of the linearization can be reduced by adding a higher number of TGA curves obtained at different heating rates. A minimum of five different heating rates TGA curves are needed when neglecting the uncertainties of the heating rate and the temperature during the calculation to obtain mean uncertainties lower than 10% for the activation energy. Nevertheless, mean uncertainties of the activation energy lower than 5% are obtained using just three TGA curves obtained at different heating rates and considering the uncertainties of the heating rate and temperature during the linearization. Finally, a sensitivity analysis was carried out to determine the effect of the temperature accuracy of the thermo gravimetric analyser employed on the final results obtained. The accuracy of the TGA device for the temperature measurement was found to have a direct effect on the uncertainties obtained for both the activation energy and the pre-exponential factor.

References

[1] R.C. Saxena, D.K. Adhikari, H.B. Goyal, Biomass-based energy fuel through biochemical routes: A review, Renew. Sust. Energ. Rev. 13 (2009) 167-178.

[2] A. Kazagic, I. Smajevic, Experimental investigation of ash behavior and emissions during combustion of Bosnian coal and biomass, Energy. 32 (2007) 2006-2016.

[3] A.E. Pütün, B. Burcu Uzun, E. Apaydin, E. Pütün, Bio-oil from olive oil industry wastes: Pyrolysis of olive residue under different conditions, Fuel Process. Technol. 87 (2005) 25-32.

[4] S. Kaewluan, S. Pipatmanomai, Potential of synthesis gas production from rubber wood chip gasification in a bubbling fluidised bed gasifier, Energy Convers. Manage. 52 (2011) 75-84.

[5] F. Orecchini, E. Bocci, Biomass to hydrogen for the realization of closed cycles of energy resources, Energy. 32 (2007) 1006-1011.

[6] M.J. Prins, K.J. Ptasinski, F.J.J.G. Janssen, Torrefaction of wood: Part 1 Weight loss kinetics, J. Anal. Appl. Pyrol. 77 (2006) 28-34.

[7] A.W. Coats, J.P. Redfern, Kinetic parameters from thermogravimetric data, Nature 201 (1964) 68-69.

[8] A. Anca-Couce, A. Berger, N. Zobel, How to determine consistent biomass pyrolysis kinetics in a parallel reaction scheme, Fuel. 123 (2014) 230-240.

[9] Z. Li, W. Zhao, B. Meng, C. Liu, Q. Zhu, G. Zhao, Kinetic study of corn straw pyrolysis: Comparison of two different three-pseudo component models, Bioresource Technol. 99 (2008) 7616-7622.

[10] T. Lin, E. Goos, U. Riedel, A sectional approach for biomass: Modelling the pyrolysis of cellulose, Fuel Process. Technol. 115 (2013) 246-253.

[11] V. Vand, A theory of the irreversible electrical resistance changes of metallic films evaporated in vacuum, Proc. Phys. Soc. 55 (1943) 222-246.

[12] K. Miura, A new and simple method to estimate $f(E)$ and $k_0(E)$ in the distributed activation energy model from three sets of experimental data, Energ. Fuel. 9 (1995) 302-307.

[13] K. Miura, T. Maki, A simple method for estimating $f(E)$ and $k_0(E)$ in the distributed activation energy model, Energ. Fuel. 12 (1998) 864-869.

[14] M. Günes, S.K. Günes, Distributed activation energy model parameters of some Turkish coals, Energy Sources Part A - Recovery Utilization and Environmental Effects 30 (2008) 1460-1472.

[15] Z. Li, C. Liu, Z. Chen, J. Qian, W. Zhao, Q. Zhu, Analysis of coals and biomass pyrolysis using the distributed activation energy model, Bioresource Technol. 100 (2009) 948-952.

[16] G. Várghegyi, P. Szabó, M.J. Antal, Kinetics of charcoal devolatilization, Energ. Fuel. 16 (2002) 724-731.

[17] Q. Wang, H. Wang, B. Sun, J. Bai, X. Guan, Interactions between oil shale and its semi-coke during co-combustion, Fuel. 88 (2009) 1520-1529.

[18] T. Wanjun, W. Cunxin, C. Donghua, 2005. Kinetic studies on the pyrolysis of chitin and chitosan, Polym. Degrad. Stabil. 87 (2005) 389-394.

[19] J.H. Yan, H.M. Zhu, X.G. Jiang, Y. Chi, K.F. Cen, Analysis of volatile species kinetics during typical medical waste materials pyrolysis using a distributed activation energy model, J. Hazard. Mater. 162 (2009) 646-651.

[20] A. Soria-Verdugo, N. Garcia-Hernando, L.M. Garcia-Gutierrez, U. Ruiz-Rivas, Analysis of biomass and sewage sludge devolatilization using the distributed activation energy model, Energy Convers. Manage. 65 (2013) 239-244.

[21] S. Hu, A. Jess, M. Xu, Kinetic study of Chinese biomass slow pyrolysis: Comparison of different kinetic models, Fuel. 86 (2007) 2778-2788.

[22] J. Cai, R. Liu, New distributed activation energy model: Numerical solution and application to pyrolysis kinetics of some types of biomass, Bioresource Technol. 99 (2008) 2795-2799.

[23] T. Sonobe, N. Worasuwannarak, Kinetic analyses of biomass pyrolysis using the distributed activation energy model, Fuel. 87 (2008) 414-421.

[24] D.K. Shen, S. Gu, B. Jin, M.X. Fang, Thermal degradation mechanisms of wood under inert and oxidative environments using DAEM methods, Bioresource Technol. 102 (2011) 2047-2052.

[25] A. Soria-Verdugo, L.M. Garcia-Gutierrez, L. Blanco-Cano, N. Garcia-Gutierrez, U. Ruiz-Rivas, Evaluating the accuracy of the Distributed Activation Energy Model for biomass devolatilization curves obtained at high heating rates, Energy Convers. Manage. 86 (2014) 1045-1049.

[26] X. Yang, R. Zhang, J. Fu, S. Geng, J.J. Cheng, Y. Sun, Pyrolysis kinetic and product analysis of different microalgal biomass by distributed activation energy model and pyrolysis-gas chromatography-mass spectrometry, Bioresource Technol. 163 (2014) 335-342.

[27] D. Chen, Y. Zheng, X. Zhu, In-depth investigation on the pyrolysis kinetics of raw biomass. Part I: Kinetic analysis for the drying and devolatilization stages, Bioresource Technol. 131 (2013) 40-46.

[28] L. Fiori, M. Valbusa, D. Lorenzi, L. Fambri, Modeling of the devolatilization kinetics during pyrolysis of grape residues, Bioresource Technol. 103 (2012) 389-397.

[29] F. Ma, Y. Zeng, J. Wang, Y. Yang, X. Yang, X. Zhang, Thermogravimetric study and kinetic analysis of fungal pretreated corn stover using the distributed activation energy model, Bioresource Technol. 128 (2013) 417-422.

[30] M. Poletto, A.J. Zattera, R.M.C. Santana, Thermal decomposition of wood: Kinetics and degradation mechanisms, Bioresource Technol. 126 (2012) 7-12.

[31] X. Yang, F. Ma, H. Yu, X. Zhang, S. Chen, Effects of biopretreatment of corn stover with white-rot fungus on low-temperature pyrolysis products, Bioresource Technol. 102 (2011) 3498-3503.

[32] J. Cai, T. Li, R. Liu, A critical study of the Miura-Maki integral method for the estimation of the kinetic parameters of the distributed activation energy model, Bioresource Technol. 102(4) (2011) 3894-3899.

[33] J. Cai, W. Wu, R. Liu, Sensitivity analysis of three-parallel-DAEM-reaction model for describing rice straw pyrolysis, Bioresource Technol. 132 (2013) 423-426.

[34] X. Liu, B. Li, K. Miura, Analysis of pyrolysis and gasification reactions of hydrothermally and supercritically upgraded low-rank coal by using a new distributed activation energy model, Fuel Process. Technol. 69 (2001) 1-12.

[35] T. Mani, P. Murugan, J. Abedi, N. Mahinpey, Pyrolysis of wheat Straw in a thermogravimetric analyzer: Effect of particle size and heating rate on devolatilization and estimation of global kinetics, Chem. Eng. Res. Des. 88 (2010) 952-958.

[36] S. Munir, S.S. Daood, W. Nimmo, A.M. Cunliffe, B.M. Gibbs, Thermal analysis and devolatilization kinetics of cotton stalk, sugar cane bagasse and shea meal under nitrogen and air atmospheres, Bioresource Technol. 100 (2009) 1413-1418.

[37] Y. Tonbul, A. Saydut, K. Yurdako, C. Hamamci, A kinetic investigation on the pyrolysis of Seguruk asphaltite, J. Therm. Anal. Calorim. 95 (2009) 197-202.

[38] M.V. Navarro, R. Murillo, A.M. Mastral, N. Puy, J. Bratroli, Application of the Distributed Activation Energy Model to biomass and biomass constituents devolatilization, AIChE J. 55 (10) (2009) 2700-2715.

[39] Y.M. Kim, S. Kim, T.U. Han, Y.K. Park, C. Watanabe, Pyrolysis reaction characteristics of Korean pine (Pinus Koraiensis) nut shell, J. Anal. Appl. Pyrol. 110 (2014) 435-441.

[40] S.S. Kim, J. Kim, Y.H. Park, Y.K. Park, Pyrolysis kinetics and decomposition characteristics of pine trees, Bioresource Technol. 101 (2010) 9797-9802.

[41] A. Aboulkas, K. El Harfi, A. El Bouadili, Pyrolysis of olive residue/low density polyethylene mixture: Part I Thermogravimetric kinetics, J. Fuel Chem. Technol. 36(6) (2008) 672-678.

[42] A. Ounas, A. Aboulkas, K. El Harfi, A. Bacaoui, A. Yaacoubi, Pyrolysis of olive residue and sugar cane bagasse: Non-isothermal thermogravimetric kinetic analysis, Bioresource Technol. 102 (2011) 11234-11238.

[43] P. Manara, D. Vamvuka, S. Sfakiotakis, A. Richel, A. Zabaniotou, Mediterranean agri-food processing wastes pyrolysis after pre-treatment and recovery of precursor materials: A TGA-based kinetic modeling study, Food Res. Int., *In Press* (2014).

[44] T.Damartzis, D. Vamvuka, S. Sfakiotakis, A. Zabaniotou, Thermal degradation studies and kinetic modeling of cardoon (Cynara cardunculus) pyrolysis using thermogravimetric analysis (TGA), Bioresource Technol. 102 (2011) 6230-6238.

[45] A.O. Aboyade, T.J. Hugo, M. Carrier, E.L. Meyer, R. Stahl, J.H. Knoetze, J.F. Görgens, Non-isothermal kinetic analysis of the devolatilization of corn cobs and sugar cane bagasse in an inert atmosphere, Thermochim. Acta 517 (2011) 81-89.

[46] P.J. Barrie, The mathematical origins of the kinetic compensation effect: 1. The effect of random experimental errors, Phys. Chem. Chem. Phys. 14 (2012) 318-326.

[47] N. Sonoyama, J. Hayashi, Characterisation of coal and biomass based on kinetic parameter distributions for pyrolysis, Fuel, 114 (2013) 206-215.

[48] J. Cai, W. Wu, R. Liu, An overview of distributed activation energy model and its application in the pyrolysis of lignocellulosic biomass, Renew. Sust. Energ. Rev. 36 (2014) 236-246.

[49] R.K. Agrawal, Compensation effect in the pyrolysis of cellulosic materials, Thermochin. Acta, 90 (1985) 347-351.

[50] J.E. White, W.J. Catallo, B.L. Legendre, Biomass pyrolysis kinetics: A comparative critical review with relevant agricultural residue case studies, J. Anal. Appl. Pyrol. 91 (2011) 1-33.

[51] E.L.K. Mui, W.H. Cheung, V.K.C. Lee, G. McKay, Compensation effect during the pyrolysis of tyres and bamboo, Waste Manage. 30 (2010) 821-830.